Refereed Proceedings

Heat Exchanger Fouling and Cleaning: Fundamentals and Applications

Engineering Conferences International *Year* 2003

Understanding and Quantifying Cleaning Processes Using Fluid Dynamic Gauging

J. Y. M. Chew
University of Cambridge

S. S. S. Cardoso
University of Cambridge

W. R. Paterson
University of Cambridge

D. I. Wilson
University of Cambridge

UNDERSTANDING AND QUANTIFYING CLEANING PROCESSES USING FLUID DYNAMIC GAUGING

J.Y.M. Chew[1], S.S.S. Cardoso[2], W.R. Paterson[3] and D.I. Wilson[4]

Department of Chemical Engineering, Pembroke Street, Cambridge, CB2 3RA, UK
E-mail: [1]ymjc2@cam.ac.uk; [2]silvana_cardoso@cheng.cam.ac.uk; [3]wrp1@cheng.cam.ac.uk; [4]ian_wilson @cheng.cam.ac.uk

ABSTRACT

Computational fluid dynamics (CFD) has been used to analyse the flow patterns generated by the fluid dynamic gauging (FDG) technique in order to allow that technology to give simultaneous measurements of fouling layer thickness and incipient strength (via breakage). Stress field predictions were generated by solving the governing Navier-Stokes equations for these quasi-laminar flows using the numerical solver *Fastlfo*™, and validated by comparison with experimental hydrostatic pressure data. Enhanced FDG was used to study the removal of a tomato paste soil, which had been characterised by Liu *et al*. (2002) using a micro-manipulation technique. Deposit strength measurements gave clear indication of increases on ageing via baking and are compared with those reported by Liu *et al*.

INTRODUCTION

The removal of unwanted fouling layers from surfaces is essential in many processes in order to restore operability, ensure hygiene or avoid cross-contamination in a multi-product environment. The efficiency of cleaning required from any cleaning process will vary from sector to sector, and this will largely dictate the technologies chosen.

A common problem across all sectors, and particularly those featuring multi-product lines, is that variations in the materials being processed result in different fouling and cleaning behaviours. The chemistry of the fouling layer must be understood in order to select appropriate cleaning chemicals, and thereafter the best mode of delivery. For example, in the dairy industry it is recognised that high surface temperature processes promote crystallisation fouling, countered by cleaning-in-place with acidic or sequestrant solutions, whereas lower temperatures yield protein-rich layers which require alkaline washes in order to swell and dissolve the deposit (Burton, 1968). Beyond the bulk chemistry factors, however, there exists opportunity for optimising cleaning cycles by selecting flow and temperature regimes to maximise cleaning rates (*e.g*. Bird and Fryer, 1991). Optimisation at this level requires knowledge of the fundamental cleaning mechanisms, of the interaction between chemistry, kinetics, transport processes and the relevant properties of the fouling material.

A further complication arises in that many fouling layers, particularly those generated in the food and biotechnology sectors, do not lend themselves readily to systematic study. Milk protein fouling layers, consisting principally of denatured β-lactoglobulin, swell in alkaline solution to form a gel of high voidage and low mechanical strength which collapses in the absence of liquid. Studying such materials in real time and in situ raises challenges which prompted the development of the technique of fluid dynamic gauging by Tuladhar *et al.* (2000) to measure thicknesses of soft layers present on surfaces in their native liquid environments. Figure 1 illustrates the principle of the gauging technique, which is based on a convergent nozzle of diameter d_t operating under suction so that liquid is drawn into the nozzle at flow rate m. The system is operated at fixed pressure difference: m is very sensitive to the clearance from the surface, h, when $h/d_t < 0.25$. This allows the surface of the soft solid to be tracked in real time, and was used by Tuladhar *et al.* (2002) to investigate the cleaning behaviour of denatured whey protein soils employed as a model for proteinaceous milk foulant.

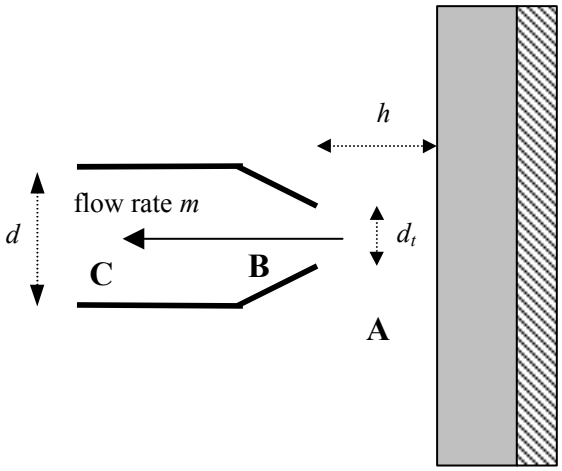

Figure 1 Dynamic gauging principle

A particular feature observed by Tuladhar *et al*. was the onset of rapid decreases in protein layer thickness at points later in the cleaning process, which were not evident in parallel measures of cleaning. Visual observation indicated that this was due to the forces imposed by the gauging flow becoming strong enough to hydro-mechanically remove the weakening layer, *i.e*. moving from a transport-controlled process to a mechanical one. This feature suggested that the dynamic gauging technique could be used to measure simultaneously the thickness and strength threshold of the

material being studied if the forces imposed by the fluid could be quantified.

A similar methodology, based on impinging laminar jets, was employed by Vaishnav and co-workers (1983) to study endothelium tissues. FDG offers advantages in not compromising the hygiene of the system and simultaneous measurement of layer thickness. This paper summarises recent work on computational fluid dynamics (CFD) calculations of the stresses imposed by gauging flows, their verification and its application to a model food soil, a tomato paste.

CFD SIMULATIONS

Fluid dynamic gauging with most aqueous solutions under quasi-stagnant conditions, *i.e*. when motion in the bulk liquid is only due to the relatively slow flow into the gauge, represents a case of a steady, laminar, incompressible and axisymmetric flow of a Newtonian fluid which is governed by the Navier-Stokes (N-S) and continuity equations. Although in the laboratory the pressure difference driving the flow is generated by a gravitational head, for CFD simulation it proves convenient to neglect gravity within the flow field and instead simply impose a chosen pressure difference to drive the flow (Tritton, 1988). Ignoring gravity, the non-dimensional N-S and continuity equations are

$$\textit{Navier} - \textit{Stokes}: \quad \mathbf{V}\cdot\nabla\mathbf{V} = -\nabla P + \frac{1}{Re}\nabla^2\mathbf{V} \qquad (1)$$

$$\textit{Continuity}: \quad div\,\mathbf{V} = \nabla\cdot\mathbf{V} = 0 \qquad (2)$$

where $\mathbf{V}$ is the dimensionless velocity vector and P is the dimensionless pressure, with

$$\mathbf{V} = \frac{1}{2v_c}\mathbf{v} \qquad (3)$$

$$\nabla = l_c\nabla^* \qquad (4)$$

$$P = \frac{p}{4\rho v_c^2} \qquad (5)$$

$$Re = \frac{2\rho v_c l_c}{\mu} \qquad (6)$$

and the subscript c implies a characteristic value. Here, l_c is the radius of the tube, v_c is the mean fluid velocity in the tube and Re the Reynolds number of the flow in the tube. A second Reynolds number based on the nozzle diameter, Re_t, can be defined and is a simple multiple of Re. These equations were solved using the Augmented Lagrangian Method (ALM) implemented by the commercial partial differential equation solver, *Fastflo*^{TM}. Spatial discretization was performed using the finite element method, with a higher concentration of mesh elements assigned in the nozzle-clearance region. Once the velocity field simulations were converged, the associated stress field was calculated. A detailed description of the CFD simulations and their verification are given in Chew *et al*. (2003). Figure 2 shows the streamlines calculated for the condition $Re_t = 120$ and $h/d_t = 0.20$. The velocity gradients are largest in the gap between the nozzle and the surface, so that localised regions of high pressure and shear stress are predicted there.

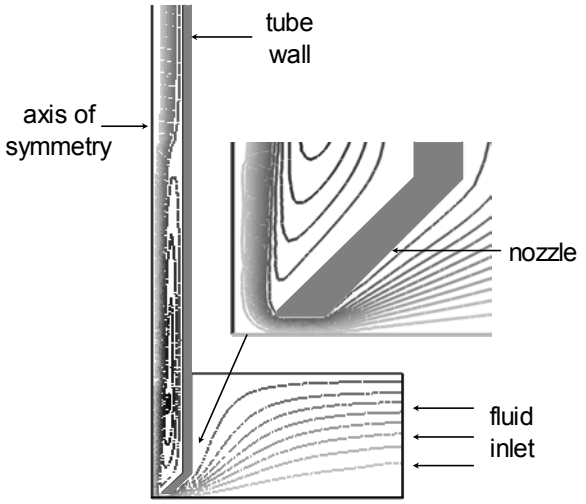

Figure 2 Calculated streamlines for gauging flow at $Re_t = 120$, $h/d_t = 0.20$

Verification

The devices previously used by Tuladhar and co-workers had featured nozzles with tube diameter d = 4 mm, so a scaled-up, geometrically similar dev ice was constructed from Perspex with d = 20 mm, mounted in a large tank. Verification experiments were performed at ambient conditions using water (viscosity = 1 mPa s) and 35 wt% aqueous sucrose solutions (viscosity = 3.7 mPa s) at different values of the driving hydrostatic head, H. The discharge flow rate, m, was measured gravimetrically and the error in all measured parameters was small. The hydrostatic pressure imposed on the surface was measured via a 0.50 mm diameter pressure tapping located in a horizontal plate across which the gauging nozzle could be traversed via a vernier scale.

Experiments proved that this large gauge reproduced the gauging characteristics obtained with smaller devices over suitably scaled operating conditions. Figure 3(*a*) shows a comparison between the simulated normal stress distributions on the gauged surface plotted with experimental results for the sucrose solution at H = 55 mm. The plots show reasonably good agreement. Other simulations proved that the presence of the measuring port on the gauged surface did not interfere with the flow in the gauge. The CFD predictions show sharp peaks in suction pressure within the inner radius of the nozzle, *i.e*. at dimensionless $R < 0.25$, where R is the dimensionless radial

coordinate with $R = 0$ being the centerline of the gauge. The experimental measurements show flatter peaks in the higher pressure region, which is partly due to the pressure tapping representing an average of the stress distribution over the exposed surface.

Figure 3(*b*) shows the associated surface shear stress distribution. The co-ordinate origin is a stagnation point: as R increases, the shear stress on the gauged surface, τ_{wall}, increases until it reaches a maximum at the radial position of the inner rim of the nozzle, and then decays rapidly to zero. The shoulder located outside the nozzle outer radius ($R \sim 0.62$) arises from inertial effects in the flow which disappear at low *Re*. For all cases considered, the peak shear stress values occurred at $R \sim 0.25$, i.e. close to the inner radius of the rim of the nozzle.

(*a*)

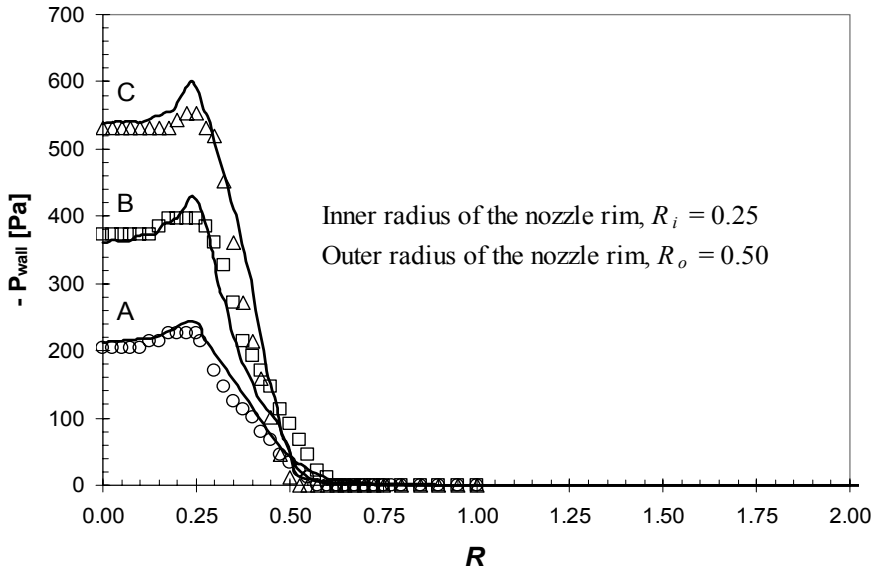

(*b*)

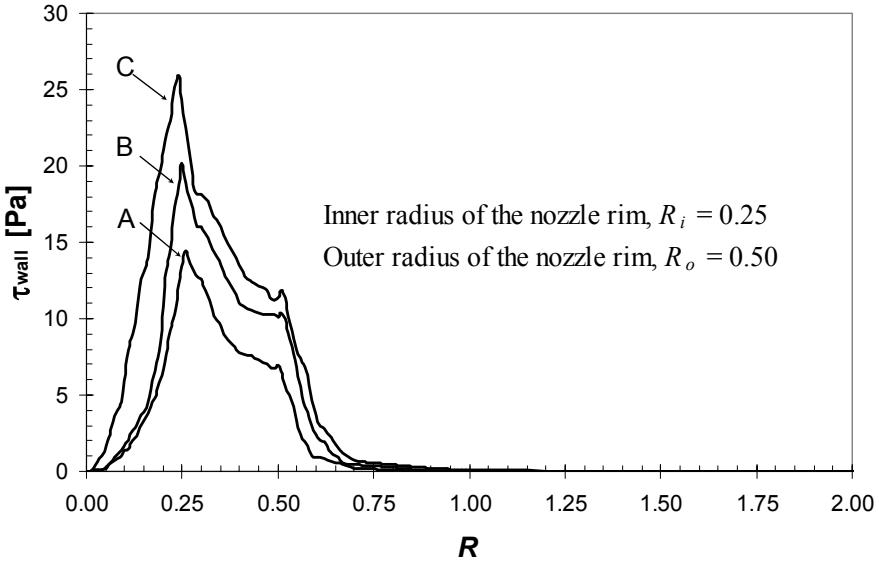

Figure 3 Stress distributions on the gauged surface for 35 wt% sucrose solution with $H = 55$ mm.
(*a*) Normal stress (hydrostatic pressure). Lines - CFD predictions; symbols - experimental measurements. A, circles - $h/d_t = 0.20$; B, squares - $h/d_t = 0.14$; C, triangles - $h/d_t = 0.10$.
(*b*) CFD calculated shear stress distributions, symbols as above.

SOIL REMOVAL STUDIES

Liu *et al*. (2002) recently reported the use of a micromanipulation technique for assessing the forces required to disrupt and remove fouling deposits. Their technique featured the use of a flat blade which was pulled through a fouling deposit located on a flat stainless steel surface, removing the deposit in the manner of a shovel clearing snow from a path. They recorded the force required to move the blade and reported this work in terms of an apparent adhesive strength. Their test material was a tomato paste product, which was baked on to stainless steel discs for a range of times and removed after different hydration periods. Noticeable ageing effects, with apparent adhesion strengths in the range 1-20 J m^{-2} were reported. Removal of tomato paste soils was therefore studied in order to compare the two techniques.

In the present work, tomato paste (composition, in wt%: 4.7 protein, 14.9 carbohydrate, 14.4 sugar, 0.4 fat, 2.0 fibre and 63.6 water) was obtained from a local supermarket and prepared in a similar manner to that reported by Liu *et al*. The paste was spread evenly (thickness ~ 2.0 mm) onto stainless steel discs to give a circular disc of soil of diameter ~ 30 mm. The samples were then heated and dried in a vacuum oven at 100°C over times ranging from 0.5-2.0 h. The structures of the tomato pastes obtained after drying were characterized by scanning electron microscopy (SEM, Philips XL 30 Series FEG) after gold/palladium sputtering (which gives better coating than gold alone). Figure 4 shows the difference in structures arising from extended baking and drying. It should be noted that the 0.5 h sample was freeze-dried before imaging in order to reduce its moisture content to a level acceptable for SEM analysis.

Samples were positioned and hydrated in water at 18°C for 1 hour prior to any gauging flow experiments. This hydration period was used as Liu *et al*. (2002) reported negligible effects of hydration on the adhesive strength of tomato paste after 1 hour. The initial thickness of the tomato paste, δ_0, was determined using the protocol outlined in Tuladhar *et al*. (2000) using low H values (typically < 20 mm) to ensure that the deposits were not deformed by the gauging flow. Water at 18°C was used as the process fluid in all soil deformation experiments.

After hydration, the gauging flow was induced. The driving force of the suction flow, H, was kept constant throughout each experiment. The vertical movement of the gauge was operated in advancing mode, *i.e*. starting from $h/d_t > 1.0$. The discharge flow rates were recorded as the gauge was moved gradually towards the sample: the time required for the deposit to reach its equilibrium thickness at different values of h/d_t was found to be less than 120 s. The behavior of the sample subject to gauging flow could also be monitored using a magnifying glass; photographs of the deposits before and after deformation were also recorded.

(*a*)

(*b*)

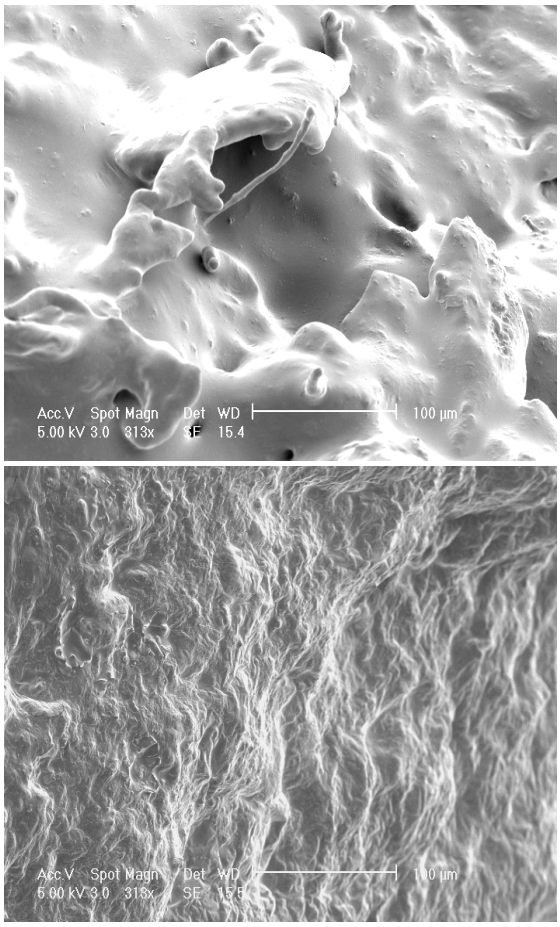

Figure 4 SEM images of tomato pastes after vacuum drying for (*a*) 0.5 h; (*b*) 2.0 h.

(*a*) (*b*)

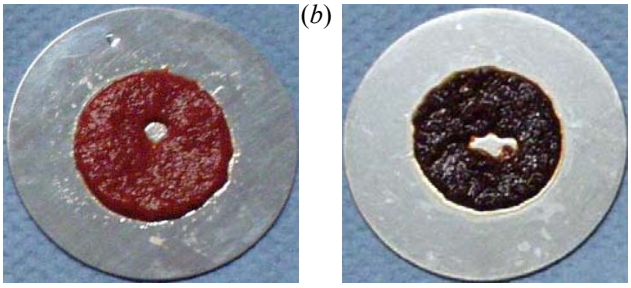

Figure 5 Tomato paste samples after FDG testing. Samples dried for (*a*) 0.5 h and (*b*) 2.0 h.

Figure 5 shows that the gauging flow generated a small crater in the deposits, which were located below the gauging axis. Visual monitoring indicated that the material failed by breakage from the stainless steel surface, with visible lumps of material being detached by the gauging flow. This result suggests that FDG will measure adhesive forces between the foulant and the equipment surface, rather

than cohesive forces within the foulant film in this case. Furthermore, it was noted that deposits generated by extended drying detached in larger pieces, whereas the most moist material – being softest – eroded away almost smoothly. This difference in brittleness is consistent with the microstructure images in Figure 4.

RESULTS AND DISCUSSION

The response of the material to imposed shear is expressed in terms of the degree of deformation, δ^*, a normalized deposit thickness, given by

$$\delta^* = \frac{\delta}{\delta_0} \tag{7}$$

where δ is the deposit thickness measured at the shear stress calculated for a given geometry and flow. The results shown represent average values for four samples at each test condition and are correlated with maximum shear stresses imposed on the surface.

Figure 6 illustrates the deformation characteristics of the hydrated baked soils. Figure 6(*a*) presents these in terms of the maximum shear stress imposed on the surface, while the manipulated variable in Figure 6(*b*) is *the suction force*, to investigate the hypothesis that deformation occurs primarily by suction. The latter was found from inspection of surface pressure plots such as Figure 3(*a*) and noting regions where the pressure deviated from the zero (hydrostatic) value. The prime assumption in determining the stresses using CFD is that any irregularity of the gauged surface does not distort the flow pattern and the stress distribution on the surface. Separate simulations indicated that small changes in surface curvature had negligible effect on flow patterns and stresses. It was also found from other experiments that the degree of roughness of the gauged surface had insignificant effect on the working principle of the gauge.

Each data set in Figure 6(*a*) shows little deformation at low shear stresses, indicating yield stress behaviour, and a transition to complete removal ($\delta^*= 0$) over a range of shear stress values. The transition is very sensitive to the extent of drying – and hence ageing and structure development. The difference in profiles between the most moist sample (drying time = 0.5 h) and others is also noteworthy, as the former exhibits a sigmoidal (possibly visco-plastic) response whereas the latter samples exhibit simple, brittle breakage at a critical value, denoted τ_y. These features are consistent with the gross removal patterns observed on the soiled discs.

The values in Figure 6(*a*) suggest that shear stresses in the order of 6 Pa would be sufficient to remove these hydrated soils. It is interesting to compare this with the shear stresses imposed by turbulent flows of aqueous solutions in typical CIP installations, given by

$$\tau_w = C_f \tfrac{1}{2} \rho u_m^2 \tag{8}$$

For a typical friction factor value of 0.005, this suggests that cleaning requires a flow velocity of the order of 1.5 m s^{-1}, which is in the region of the range of 1-2 m s^{-1} often quoted for CIP, based on Timperley (1991). It should be noted, however, that Liu *et al*.'s results for tomato paste showed a reduction of apparent adhesive strength to approximately 1/2 or 1/3 of the original values over the initial 30 minutes of hydration, and an increase in this strength of six-fold over baking times ranging from 0 to 4 h, so that extensive soaking would be required before these flow velocities were able to remove the aged soils.

The effect of ageing is also evident in Figure 6(a), with τ_y increasing progressively over bake time, approaching an asymptote of 14 Pa after 3 h. This trend mirrors that reported by Liu *et al*. remarkably closely, although they reported a six-fold change in apparent adhesive strength. The asymptotic behaviour is consistent with the development of new bonds as a result of the chemical changes which occur on extended heating, namely caramelisation of sugars, denaturation of protein and polymerization of fat (Cheow and Jackson, 1982).

A correlation plot for the two parameters is presented in Figure 7. The relationship is almost perfectly linear (regression coefficient, R^2 = 0.998) but does not pass through the origin, indicating that different physical processes are involved in the two measurements. Direct numerical comparison of the apparent adhesive strength measured by micro-manipulation and the critical shear stress required to remove the deposit obtained from FDG studies is not straightforward as a deformation model is required. The micro-manipulation action involves moving material away from the rupture plane, and if the material is cohesive or highly viscous, this will require additional work which will be manifested in the measured forces. Relating the shear stress measurements to the apparent adhesive energy (work of deformation) is strongly model-dependent. An alternative, initial, approach is to compare the forces reported in the micro-manipulation studies, where a 30 mm wide probe of 1 mm thickness was pulled across stainless steel discs of diameter 26 mm coated with deposit. The force profile reported by Liu *et al*. exhibited a maximum value of order 200 mN when the probe was half-way across the sample. If the work done is localised to the region under the probe, and the force against which the probe moves is given by the critical yield stress, say 10 Pa (other material being assumed to move out of the way in a low cohesion manner), an estimate of the force required is

force = stress × area = 10 × 0.026 × 0.001 = 260 μN

which is three orders of magnitude less than that reported. An alternative model is to assume that the whole deposit

layer shears during micro-manipulation and the probe senses the force required to move the sheared disc of material off the plate. This is a very crude model, but would give an estimate of the force of 5 mN, again significantly smaller. Furthermore, the reported deposit removal behaviour and force profiles are not consistent with this failure mode.

(*a*)

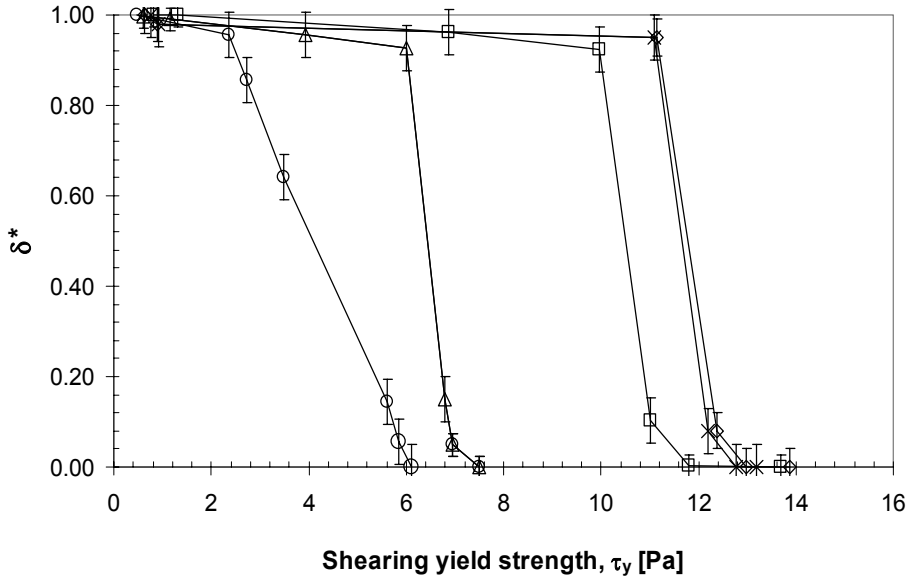

(*b*)

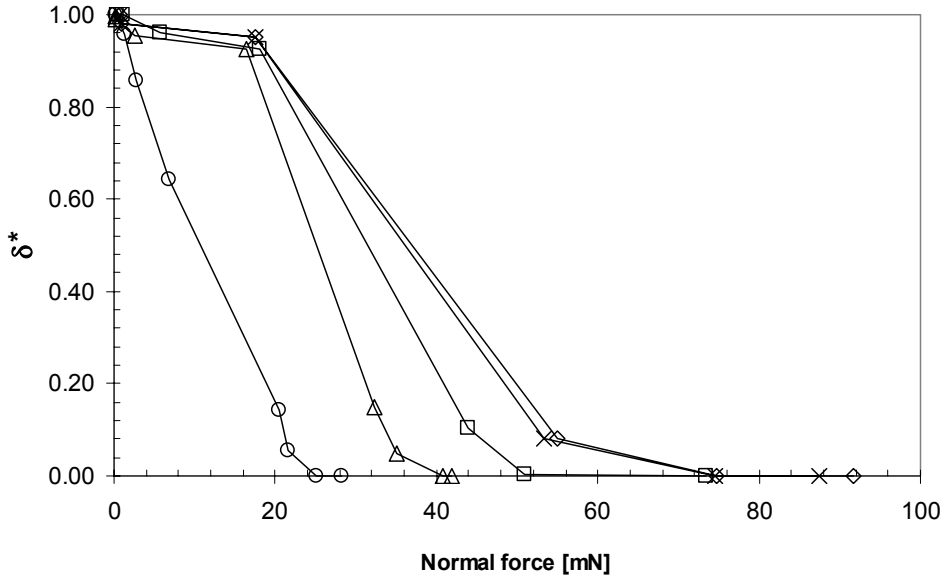

Figure 6 Deformation behaviour in response to stresses imposed by gauging flow.
(a) Maximum in surface shear stress: (b) normal suction force imposed on film.
Drying time – 0.5 h (circles), 1.0 h, (triangles), 2.0 h (squares), 3.0 h (crosses), 4.0 h (diamonds).

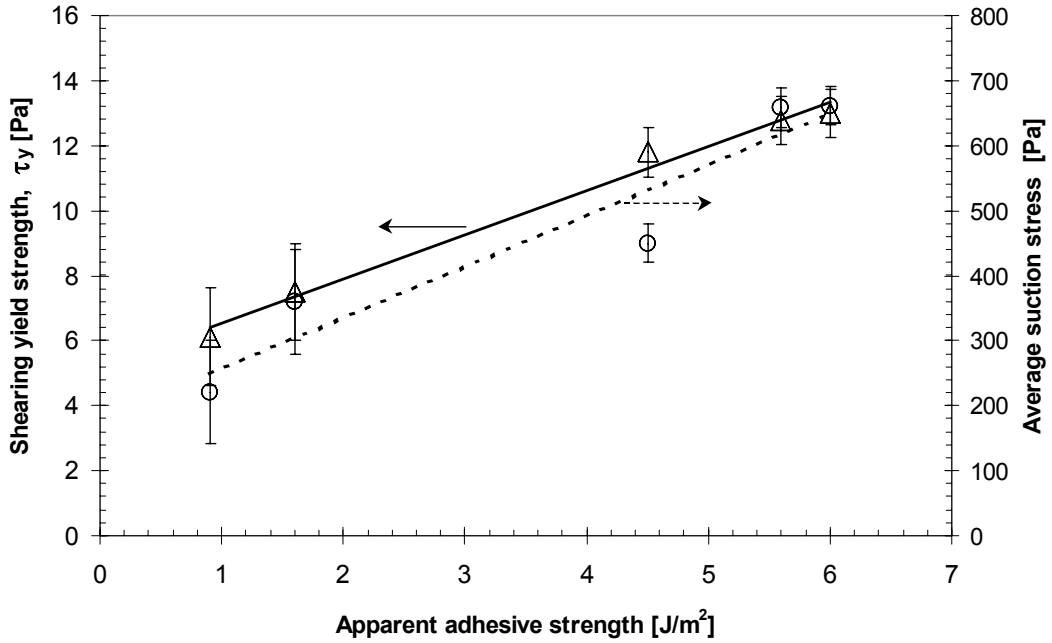

Figure 7 Correlation between shearing yield strength of tomato paste measured in this work and the corresponding apparent adhesive strength data obtained from micro-manipulation studies by Liu et al. (*2002*). Symbols – triangles, shearing yield strength; circles, average normal (suction) stress.

The characteristics evident in Figure 6(*b*), where deformation is presented in terms of suction, are slightly different and indicate that the two failure modes are not equivalent. The most moist sample exhibits deformation under even the lowest value of applied suction stress and decays linearly, whereas the other samples exhibit a common threshold force of ~ 20 mN, which corresponds to an average suction pressure of 200 Pa. It is noteworthy that this force would be sufficient to remove most of the moist layer. Imposing larger forces on the aged materials removes most of the material, and the force required to remove the last fraction is a strong function of bake time. Interpreting the results in this manner suggests some heterogeneity in the deposits, and a possible transition from cohesive failure in the bulk material to adhesive failure with the surface layer.

Figure 7 shows that the average suction stress (and normal force) scales similarly well with Liu *et al.*'s adhesion strength (regression coefficient, R^2 = 0.92). Scaling the FDG values to the micro-manipulation by relating suction strength to cohesive strength underestimates the traction force required, again suggesting that micromanipulation involves extra deformation work.

The contrasting interpretations of these FDG results, of shear vs. suction deformation and failure, require further investigation to confirm the mechanism involved. One method under consideration is to reverse the flow, generating equivalent shear but hydrostatic compression.

These results illustrate how recognition of the difference in deposit breakdown modes is important. Removal of some soils will be dominated by *cohesive* processes, whereby shear imposed by the cleaning fluid breaks down and progressively erodes the foulant matrix, whereas others will feature adhesive effects, where the principal plane of weakness occurs between the foulant and the surface of the process equipment. One avenue for further development is to apply the micro-manipulation and FDG techniques to identical materials in order to elucidate the differences in removal parameters.

The dynamic gauging technique has thus been validated for measurement of stresses causing significant deformation of fouling deposits in situ and in conditions related to the native environment. It is noteworthy that the peak shear stresses generated in Figure 3(*b*), of order 20 Pa, correspond to those found in steady turbulent flows of CIP solutions, indicating that this technique allows one to study the effect of physical (hydraulic) removal processes under otherwise quiescent or laminar flow conditions, at considerable space and resource saving.

Direct estimation of the stresses acting on swollen whey protein gels in the studies by Tuladhar *et al*. (2002) is not immediately possible as that work featured bulk duct flows, which introduces convective components into, and reduces the symmetry of, the CFD simulations. However, the quasi-stagnant simulations indicate that the stresses

would be comparable with those imposed by turbulent flows. Further CFD work is required to permit reliable estimation of the stress field for FDG in duct flows.

One area where the measurement of adhesive interactions, *i.e*. between deposits and surfaces, is of particular importance is in the characterisation of antifouling surfaces - where foulant nuclei cannot adhere permanently, or in anti-deposition (removal) - where sustained growth of deposit does not occur because of progressive erosion of foulant or fouling colonies. The classical Kern-Seaton (1959) model for fouling behaviour includes an anti-deposition term which is often expressed as some function of shear stress. Foulant deformation characteristics obtainable using this enhanced FDG technique can now be used to construct models for fouling removal terms. Initial investigations on mineral calcium scales, performed recently in collaboration with the Technical University of Braunschweig, Germany, have proved very promising (data not reported): this work continues.

CONCLUSIONS

Application of the technique of fluid dynamic gauging has been significantly augmented by CFD studies of the quasi-stagnant gauging flows which now allow the stress field imposed on the surface under investigation, by Newtonian liquids, to be quantified with a reasonable degree of accuracy. The numerical simulations obtained with the *Fastflo*^{TM} solver were confirmed by hydrostatic pressure measurements over a range of liquid viscosities and densities. Particular features of note were that the surface shear stress is largest in the area directly underneath the gauging nozzle rim, and that shear stresses characteristic of turbulent CIP systems could be generated in these quasi-stagnant systems by judicious selection of suction head and clearance between the gauging nozzle and the surface, h/d_t.

Application of this enhanced FDG technique has been demonstrated using tomato paste soils, baked on to stainless steel discs and then hydrated, simulating the micro-manipulation studies by Liu *et al*. (2002). The critical shearing yield stress for the soil was found to be strongly dependent on the extent of baking (ageing) of the deposit, approaching an asymptote as the material was transformed from a soft, malleable paste into a hard, brittle semi-solid. Precise interpretation of the yield mechanism, *i.e.* shear vs. suction for these soft materials, requires further work. The ageing characteristics reflected the trends reported by Liu *et al*. very well, although the numerical values could not be directly compared.

ACKNOWLEDGEMENTS

JYMC wishes to acknowledge support from the Cambridge Commonwealth Trust. Grants to allow DIW to travel and attend the conference, from Jesus College, Cambridge, and the University are both gratefully acknowledged. SEM investigations were assisted by Mr. Tony Burgess (Department of Anatomy).

NOMENCLATURE

C_f	Fanning friction factor
d	gauging tube diameter, m
d_t	nozzle diameter, m
h	clearance, m
H	hydrostatic head, m
l_c	radius of tube, m
m	discharge mass flow rate, kg s^{-1}
P	pressure, Pa
R	dimensionless radius, = r/l_c
Re, Re_t	Reynolds number, based on nozzle diameter
u_m	mean velocity, m s^{-1}
$\boldsymbol{V}$	velocity vector, m s^{-1}
v_c	mean velocity of fluid in tube, m s^{-1}
δ_0	deposit thickness, initial value, m
δ^*	normalized deposit thickness
μ	viscosity, Pa s
ρ	density, kg m^{-3}
τ_{wall}	wall shear stress, Pa
τ_y	critical shearing yield stress, Pa

REFERENCES

Burton, H. 1968, Deposition from whole milk in heat treatment plant – A review and discussion, *J. Dairy Res*. Vol. 35, 317-330.

Bird, M.R. and Fryer, P.J. 1991, An experimental study of the cleaning of surfaces fouled by whey proteins, *Trans.IChemE*, Vol. 69C, 13-21.

Chew, J.Y.M., Cardoso, S.S.S., Paterson, W.R. and Wilson, D.I., 2003, CFD studies of dynamic gauging, *Chem. Eng. Sci.*

Cheow, C.T. and Jackson, A.T., 1982, *J. Food Tech*., Vol. 17, 417-430.

Kern, D.Q. and Seaton, 1959, A theoretical analysis of thermal surface fouling, *Brit.Chem Engng*., Vol. 4, 256-262.

Liu, W., Christian, G.K., Zhang, Z. and Fryer, P.J. (2002) Development and use of a micromanipulation technique for measuring the force required to disrupt and remove fouling deposits, *Trans.IChemE.*, Vol. 80C 286-291.

Timperley, D.A., 1989, Cleaning in place, *J Soc. Dairy Technology*, Vol. 42(2), 32-33.

Tuladhar, T.R., Paterson, W.R., Macleod, N. and Wilson, D.I., 2000, Development of a novel non-contact proximity gauge for thickness measurement of soft deposits and its application in fouling studies, *Can.J.Chem.Eng*., Vol. 78, 935-947.

Tuladhar, T.R., Paterson, W.R. and Wilson, D.I, 2002, Investigation of alkaline cleaning-in-place of whey protein deposits using dynamic gauging, *Trans.IChemE.*, Vol. 80C, 199-214.

Vaishnav, R.N, Patel, D.J, Atabek, H.B, Deshpande, M.D, Plowman, F., and Vossoughi, J. (1983). Determination of the local erosion stress of the canine endothelium using a jet impingement method. *J.Biomech. Eng.,* Vol. 105, 77-83.